Strategic control of location and ordinal context in visual working memory

Jacqueline M. Fulvio[1], Qing Yu[2,3], & Bradley R. Postle[1,2]

[1]Department of Psychology, University of Wisconsin–Madison

[2]Department of Psychiatry, University of Wisconsin–Madison

[3]Institute of Neuroscience, Center for Excellence in Brain Science and Intelligence Technology, Chinese Academy of Sciences

Corresponding author:

Jacqueline M. Fulvio, PhD

1202 West Johnson St.

Madison, WI 53706-1611

(608) 262-1040

jacqueline.fulvio@wisc.edu

RUNNING TITLE: Strategic control of context in working memory

Abstract (200 words)

Working memory requires encoding stimulus identity and context (e.g., where or when it was presented). To explore the neural bases of the strategic control of context binding in working memory, we acquired fMRI while subjects performed delayed recognition of three orientation patches presented serially and at different locations. The recognition probe was an orientation patch with a superimposed digit, and depending on pretrial instruction subjects responded according to the probe's location (*location-relevant*), the ordinal position corresponding to its digit (*order-relevant*), or just its orientation (*context-irrelevant*). Delay-period signal in PPC was greater for context-relevant than for *context-irrelevant* trials, and multivariate decoding revealed strong sensitivity to context binding requirements (relevant vs. *irrelevant*) and to critical domain of context (*location-* vs. *order-relevant*) in both occipital cortex and PPC. At recognition, multivariate inverted encoding modeling revealed markedly different patterns in these two regions, suggesting different context-processing functions. In occipital cortex, an active representation of the location of each of the three samples was reinstated, regardless of trial type. The pattern in PPC, in contrast, suggested a filtering of location-context information that was dependent upon trial type. These results indicate that PPC exerts strategic control over the representation of location context in visual working memory.

Keywords: context-binding, control, fMRI, parietal cortex, visual working memory

Introduction

Several recent studies have provided evidence that delay-period activity in the intraparietal sulcus (IPS) reflects, at least to some extent, context-binding operations (Cai et al. 2019; Cai et al. 2020; Gosseries, Yu, et al. 2018), thus offering a complement to the idea that this activity reflects stimulus representation in visual working memory (VWM; Bettencourt & Xu 2016; Todd & Marois 2004; Xu 2017; Xu & Chun 2006). Gosseries, Yu, et al. (2018) sought to dissociate activity related to context-binding demands from that related to memory load, per se, by varying stimulus category homogeneity within the memory set. In addition to trials requiring delayed recall of the direction of motion of one dot-motion patch ("*1M*"), subjects also performed two types of load-of-three trials: memory for three motion patches ("*3M*"); and memory for one motion patch and two color patches ("*1M2C*"). Items were presented serially, and a digit in the middle of the response dial indicated which sample (the first, second, or third) was to be recalled. Thus, remembering ordinal context was critical for *3M* trials, but much less so for *1M2C* trials, for which the ordinal position of only one of the two color patches needed to be retained. Delay-period activity in IPS was elevated for *3M* trials relative to *1M2C* and *1M* trials, which themselves did not differ.

Cai et al. (2020) used a logic similar to that of Gosseries, Yu, et al. (2018), but used location as the critical dimension of context instead of ordinal position: sample items could appear in four possible locations, and trials required delayed recall of one oriented bar ("*1O*"), of one from a set of three simultaneously presented oriented bars ("*3O*"), or of one item from a set of one orientated bar, one color patch, and one luminance patch ("*1O1C1L*"). For all trial types, the location at which the response dial appeared matched the location of the sample item to be recalled. However, because the orientation, color, and luminance response dials only afforded a

response to one kind of stimulus domain, the context-binding demands on *1O1C1L* trials were negligible. As was the case with Gosseries, Yu, et al. (2018), delay-period activity in IPS was markedly higher for trials with high context-binding demand (i.e., *3O*) relative to *1O* and to *1O1C1L* trials, which did not differ (Cai et al. 2020).

Because the above-summarized studies provided evidence for a role for IPS in context-binding for both spatial location and ordinal position, an important question to address is whether the same areas of IPS are involved in the processing of context from both of these domains. A second important question is whether context-binding in VWM can be strategically controlled according to task demands. An alternative, implied in results from a different set of analyses not reviewed here (Cai et al. 2019), raises the possibility that location context may be encoded obligatorily into WM, even when it is task irrelevant.

To address these questions, we investigated context binding in a task in which the stimulus content (three orientation patches) and presentation (serial presentation at three different locations) were identical across conditions, and a pre-trial instructional cue indicated whether location context, ordinal context, or neither was required to interpret the memory probe. The study design was preregistered (https://osf.io/gc9m4/?view_only=c243e13b59294a06bd299b6d06c63a1c) after functional magnetic resonance imaging (fMRI) scanning of three pilot subjects confirmed that our design was practical. Here, we report the results from the preregistered analyses (including "additional planned analyses"), as well as from post hoc exploratory analyses that follow up on the findings from the former. To preview, the preregistered hypotheses focused on three sets of analyses in two brain regions of primary interest, parietal and occipital cortex (named *parietal-delay* ROI and *occipital-sample* ROI, respectively): The first set of analyses (Hypothesis 1) examined

univariate changes in fMRI signal intensity modulated by context-binding demands; the second set of analyses (Hypothesis 2) examined multivariate activity patterns that discriminated between conditions with varied context-binding demands; and the third set of analyses (Hypothesis 3) examined neural representations of location context using multivariate inverted encoding modeling (IEM). In addition to these focused hypothesis tests, we also planned to carry out whole-brain analyses related to *Hypotheses 1* and *2*, and follow-ups to *Hypothesis 3* using different procedures for training IEMs. Finally, after these analyses were carried out, results related to *Hypothesis 3* prompted us to carry out post hoc exploratory analyses.

Preregistered hypotheses

Hypothesis 1 (univariate analyses)

Hypothesis 1A: Late delay-period fMRI signal intensity (at 10-14s; TRs 6-7) in the *parietal-delay* ROI will be modulated by context-binding demands, with greater signal intensity for context-relevant trials compared *context-irrelevant* and load-of-1 trials.

Hypothesis 1B: Late delay-period fMRI signal intensity in the *occipital-sample* ROI will not be modulated by context-binding demands, with signal returning to baseline in all four trial types.

Hypothesis 1C: Late delay-period fMRI signal intensity will not differ between location-context and ordinal-context trials, in either the *parietal-delay* ROI or the *occipital-sample* ROI.

Hypothesis 2 (multivariate pattern analyses)

Hypothesis 2A: Multivariate pattern analysis (MVPA) of activity in the *parietal-delay* ROI will be successful in discriminating context-relevant from *context-irrelevant* conditions (i.e., [(*location-relevant* + *order-relevant*) versus *context-irrelevant*] trials) during all three epochs of the trial.

Hypothesis 2B: MVPA of activity in the *occipital-sample* ROI will be successful in discriminating context-relevant from *context-irrelevant* conditions (i.e., [(*location-relevant* + *order-relevant*) versus *context-irrelevant*] trials) during all three epochs of the trial.

Hypothesis 2C: MVPA of activity in the *parietal-delay* ROI will be successful in discriminating *location-relevant* from *order-relevant* trials during all three epochs of the trial.

Hypothesis 2D: MVPA of activity in the *occipital-sample* ROI will be successful in discriminating l*ocation-relevant* from *order-relevant* trials during all three epochs of the trial.

Hypothesis 3 (inverted encoding modeling)

Hypothesis 3A: Multivariate inverted encoding modeling (IEM) of activity in the *occipital-sample* ROI will produce robust reconstructions of the probe location (TRs 9 and 10) from load-of-3 trials when trained on data corresponding to the sample location-evoked signal (TR 4) of load-of-1 trials, for all load-of-3 trial types.

Hypothesis 3B: At probe (TRs 9 and 10), IEM reconstruction of the location of the sample corresponding to the digit will be significantly different from the IEM reconstruction of the location of the probe in the *occipital-sample* ROI activity.

Hypothesis 3C: At probe (TRs 9 and 10), IEM reconstruction of the location of the uncued sample will be significantly different from the IEM reconstruction of the location of the probe in the *occipital-sample* ROI activity.

Materials and Methods

Subjects

Estimated effect sizes for the preregistered study were based on data from previous experiments by our group (Gosseries, Yu, et al. 2018; Cai et al. 2020*;* Yu, Teng, & Postle 2020).

Power analyses based on the results of those studies indicated that we would need data from 15 subjects to achieve 90% power to detect the effects predicted by Hypotheses 1-3. Subjects who met the following inclusion criteria were enrolled in the order in which they volunteered: being 18-35 years in age, right-handed, having normal or corrected-to-normal vision, reporting no history of neurological disease, seizures, or fainting, of a history chronic alcohol consumption or of psychotropic drugs, and having no contraindications for MRI scanning. Subjects who were able to achieve an accuracy of 83% correct or higher in each of the three context-binding conditions (see *Load-of-3 trials*, below, for details) for at least one of six 18-item training blocks administered during a behavioral training/screening session were invited to continue in the fMRI portion of the study. Subjects with fMRI datasets deemed unusable were replaced, and data collection continued until 15 usable datasets were obtained.

34 individuals completed the behavioral training/screening session with the performance of 23 of those individuals qualifying for the fMRI portion of the study. 20 total were scanned, with data from 5 subjects deemed unuseable due to excessive errors and/or missed responses (n=2), completion of only one of the two scanning sessions (n=2), or findings of clinical relevance in the anatomical scan (n=1). The final sample of 15 included 9 females / 6 males, aged 18 – 34 years (*M* = 21.6 years; *SD* = 4.1 years). We note that this final sample was collected after study preregistration and therefore does not include the three pilot participants upon whose data the preregistration was based. The Human Subjects Institutional Review Board of the University of Wisconsin-Madison approved the study protocol, and all participants provided informed consent.

Visual stimuli and behavioral tasks

Load-of-3 trials

The stimuli consisted of sinusoidal gratings. The contrast of the gratings was held constant at 0.6 and the spatial frequency was 1 cycle/deg, phase angle varying randomly between 0 deg and 179 deg for each presentation. The gratings were presented within a circular patch with a 4 deg diameter, at one of six locations around a central fixation circle (156 pixels in diameter). Probe stimuli consisted of a grating with a superimposed digit centered in the patch (40 pixels in height), rendered in red. The six stimulus locations were positioned at seven degrees eccentricity from fixation at angles of 0 deg, 60 deg, 120 deg, 180 deg, 240 deg, and 300 deg (see **Figure 1A** for a schematic of the stimulus configuration). For each presentation, the gratings were randomly assigned one of six orientation values: 10 deg, 40 deg, 70 deg, 100 deg, 130 deg, or 160 deg. The cardinal orientations were not included in the set to reduce the likelihood of verbal encoding. All stimuli were generated and presented in MATLAB (MathWorks) and Psychtoolbox-3 (http://psychtoolbox.org; Brainard 1997; Pelli 1997; Kleiner et al. 2007).

Each trial of the delayed-recognition task began with an instructional cue that identified the trial type – *location-relevant* (a "location pin" icon), *order-relevant* ("#"), or *context-irrelevant* ("*") – followed by the serial presentation of three sample stimuli (500 ms presentation, 250 ms inter-stimulus interval (ISI)), each appearing at a different location. After an 8-second delay, a probe stimulus (oriented grating with same properties as the sample stimuli, but with a superimposed digit rendered in red) appeared for 4 sec, and a "match" or "nonmatch" response was required while the probe remained on the screen. Feedback (green fixation dot = correct; red fixation = incorrect or time-out) was provided for the first sec following probe offset, after which the fixation dot was black for the remaining 7-sec of the ITI (**Figure 1B**). On *location-relevant* and *order-relevant* trials, the probe appeared in one of the three locations

where a sample had appeared, and the superimposed digit was “1”, “2”, or “3”. On *location-relevant* trials, the probe’s location was the same as the sample against which it should be compared, whereas on *order-relevant* trials the digit indicated the ordinal position of the sample (i.e., the one that appeared first, second, or third) against which it should be compared. On these two trial types, the value of the irrelevant dimension was selected at random from the remaining samples, meaning that the probe’s location and digit never cued the same sample. On *context-irrelevant* trials the probe stimulus appeared at one of the three locations that had not been occupied by a sample and the superimposed digit was randomly chosen from the set of “4”, “5”, and “6” (i.e., neither corresponded to any of the samples), and the subject was to indicate if the probe orientation matched that of any of the three samples (**Figure 1B**). For each trial type, the orientation of the probe matched the orientation of the critical sample(s) on 50% of the trials. Subjects responded via button press on the keyboard (“1” for match, “2” for non-match).

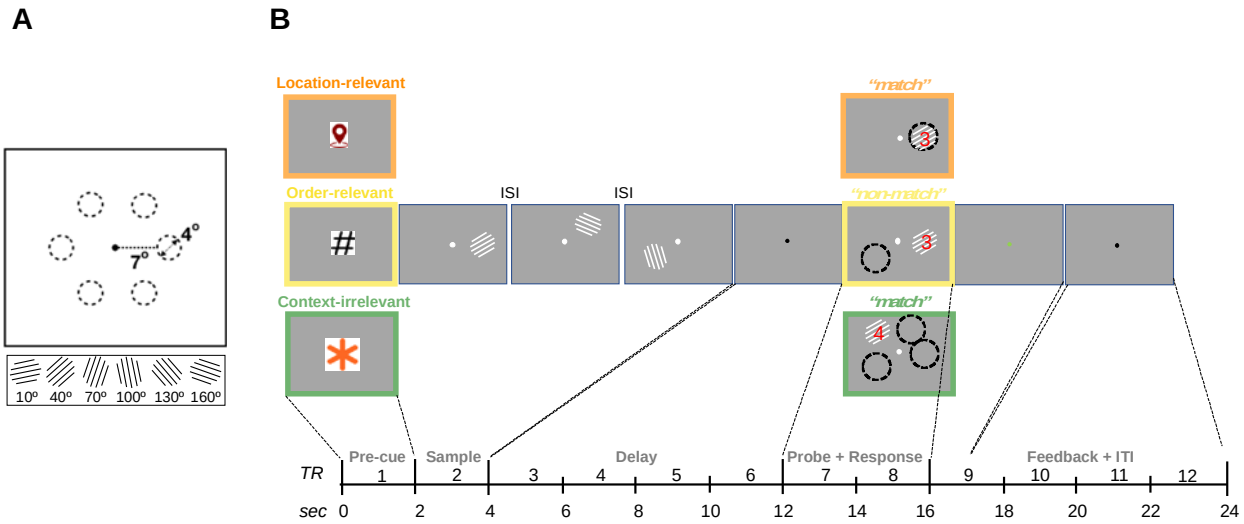

Figure 1. Experimental paradigm. (**A)** Sample stimuli consisted of oriented-grating patches (4 deg diameter) drawn from a fixed set of six values and presented at three from a fixed set of six equally-spaced locations, each at 7 deg eccentricity relative to a central fixation point. **(B)** The primary task comprised three interleaved trial types that each began with a pre-cue indicating trial type. The pre-cue was followed by the presentation of three sample gratings of different orientations, presented serially, each at a different location. After an 8-second delay period, the probe stimulus appeared. The basis for the recognition decision was determined by the trial type: on location-relevant trials, subjects compared the orientation of the probe to their memory of the orientation of the sample item that had appeared at the location occupied by the probe; on order-relevant trials, subjects compared the orientation of the probe to their memory of the orientation of the sample item that occurred in the ordinal position indicated by the superimposed digit; on context-irrelevant trials, subjects compared the orientation of the probe to their memory of all three sample item orientations. For illustration purposes, this figure uses dashed circles to illustrate the location of the sample(s) being tested; these did not appear during the experiment.

Load-of-1 trials

The stimuli and procedure for the load-of-1 trials were similar to those of the load-of-3 trials, with three exceptions: No precue was presented; the 500 ms presentation of the single sample item was followed by an 8.5-second delay, and the recognition probe consisted solely of a grating (i.e., no digit) and always appeared at the same location as had the sample.

Experimental procedures

Behavioral training/screening session

The behavioral training/screening session took place on a separate day prior to fMRI scanning. It began with a block of 18 load-of-1 trials to familiarize subjects with the delayed recognition task. The session continued with six blocks of 18 load-of-3 trials. Subjects achieving an accuracy of 83% or above in each of the three context conditions (i.e., *location-relevant*, *order-relevant*, *context-irrelevant*) in at least one of the load-of-3 blocks were invited to participate in the fMRI sessions, which took place on the soonest dates afforded by the subject's and scanner availability. Enrollment continued until the planned sample of 15 subjects completed both fMRI sessions and the data for the sample were all deemed useable (i.e., they were free of significant artifacts and other image quality concerns).

fMRI sessions

The behavioral tasks completed during fMRI scanning were identical to those the subject completed during the behavioral training/screening session. The experimental stimuli were presented using a 60-Hz projector (Silent Vision 6011; Avotec) and viewed through a coil-mounted mirror. The viewing distance was 68.58 cm and the screen width was 33.02 cm. fMRI scanning occurred in two sessions per subject. The first fMRI session consisted of eight 18-trial runs of load-of-3 trials followed by five 18-trial runs of load-of-1 trials. Each run lasted for 7

minutes and 20 seconds. The second fMRI session consisted of seven 18-trial runs of Load-of-3 trials followed by five 18-trial runs of load-of-1 trials. The two sessions combined yielded a total of 270 load-of-3 trials (90 per context-binding trial type; 15 per location per context-binding trial type) and a total of 180 load-of-1 trials (30 per location). Responses were given via button press using two buttons on an MR-compatible 4-button box. The buttons corresponding to a 'match' or 'non-match' response were swapped and counterbalanced between subjects.

Whole brain images were acquired with a 3-T MRI scanner (Discovery MR750; GE Healthcare) at the Lane Neuroimaging Laboratory at the University of Wisconsin–Madison. For all subjects, a high-resolution T1-weighted image was acquired with a fast-spoiled gradient-recalled echo sequence [repetition time (TR) 8.2 ms, echo time (TE) 3.2 ms, flip angle 12°, 172 axial slices, 256 x 256 in-plane, 1.0 mm isotropic]. A T2*-weighted gradient echo pulse sequence was used to acquire data sensitive to the BOLD signal while subjects performed the delayed recognition task (TR 2,000 ms, TE 25 ms, flip angle 60°, within a 64 x 64 matrix, 40 sagittal slices, 3.5 mm isotropic). Each of the 25 fMRI scans generated 220 volumes. Eye movements were monitored using a ViewPoint EyeTracker system (Arrington Research).

fMRI data were preprocessed using the Analysis of Functional Neuroimages (AFNI) software package (https://afni.nimh.nih.gov; Cox 1996). Each run began with eight seconds of dummy pulses to achieve a steady state of tissue magnetization before task onset. All volumes were spatially-aligned to the first volume of the first run using a rigid-body realignment and then aligned to the T1 volume. Volumes were corrected for slice-time acquisition, and linear, quadratic, and cubic trends were removed from each run to reduce the influence of scanner drift. For univariate analyses, data were spatially smoothed with a 4-mm full-width at half-maximum Gaussian and z-scored separately within run for each voxel. For multi-voxel pattern analyses

(MVPA) and inverted encoding modeling (IEM), data were z-scored separately within runs for each voxel, but the data were not smoothed. All analyses were carried out in each subject's native space.

Univariate analyses entailed calculating the percentage signal change in BOLD activity relative to baseline for each time point during the delayed-recognition task. The average BOLD activity of the first TR of each trial was used as baseline. A conventional mass-univariate general linear model (GLM) analysis was implemented in AFNI, with sample, delay, and probe periods of the task modeled with boxcars (2 s, 8 s, and 4 s in length, respectively) convolved with a canonical hemodynamic response function (HRF). Differences in BOLD activity from baseline were evaluated with one-sample *t*-tests and Bayes factors of the likelihood of the different-from-baseline alternative vs. not-different-from-baseline null hypothesis.

To generate regions of interest (ROIs), we followed the approach used by Gosseries, Yu, et al. (2018) and Cai et al. (2019), and focused our analyses on two anatomically constrained functional ROIs: an *occipital-sample* ROI and a *parietal-delay* ROI. The *occipital-sample* ROI was defined as the 500 voxels displaying the strongest loading on the contrast [sample – baseline] from the GLM, collapsed across the three context-binding conditions in the load-of-3 trials, and located within the anatomical mask for occipital cortex from the Talairach Daemon atlas for AFNI transformed to each subject's individual structural image via affine transformations (Jenkinson & Smith 2001), and further refined via nonlinear interpolation (Andersson et al. 2007). The *parietal-delay* ROI was defined as the 500 voxels displaying the strongest loading on the contrast [delay – baseline], also collapsed across the three context-binding conditions and located within an anatomical mask for parietal cortex from the Talairach

Daemon atlas for AFNI transformed to each subject's individual structural image using the same procedures as used for defining the standard occipital mask.

In addition to the ROI generation described above, we also defined anatomical ROIs for subregions of the intraparietal sulcus (IPS0-IPS5) based on the Wang et al. (2015) probabilistic atlas, and selected the 500 most responsive voxels within each (see Gosseries, Yu, et al. 2018). This approach allowed more granularity in some of the tests of the activity related to context-binding demands in IPS.

Data analysis

Analysis of behavioral data

Behavioral performance during the fMRI portion of the study was analyzed for accuracy and reaction time. Accuracy was quantified as percentage of trials in which a correct response ('match' or 'non-match') was given. Accuracy in each of the four trial types was tested against the chance performance level of 50% using one-tailed, one-sample *t*-tests. Two-tailed paired-sample *t*-tests were used to test for differences between conditions. Both within-subject and between-subject reaction times were assessed as median reaction times due to positive skew in the distributions. 95% confidence intervals for the median between-subject reaction times were obtained with a bias-corrected and accelerated (BCa) bootstrapping procedure with 10,000 iterations, implemented using the *BCa_bootstrap.m* MATLAB function (Van Snellenberg 2018). Two-sided sign tests using the exact method for obtaining the *p*-value were used to test for differences in median reaction times between conditions.

Implementation of a priori hypothesis tests

Hypothesis 1 was motivated by the idea that delay-period load sensitivity of activity in posterior parietal cortex may reflect, at least in part, the demands on context binding that often

covary with memory load (Gosseries, Yu, et al. 2018; Cai et al. 2019; Cai et al. 2020). Its tests were implemented with univariate analyses that tested for task vs. baseline and context-relevant vs. *context-irrelevant* differences in late-delay period BOLD (TRs 6-7), via one-sample *t*-tests and Bayes factors of the likelihood of the conditional differences (alternative) hypothesis vs. no differences (null) hypothesis.

Hypothesis 2 assessed evidence that patterns of activity in brain areas associated with VWM would be sensitive to (i) the level of demand on context binding, and (ii) the informational domain of task-specific context. To test this, we carried out trialwise category-level multivariate voxel pattern analysis (MVPA) to discriminate activity observed on (i) context-relevant vs. *context-irrelevant* trials; and (ii) *location-relevant* vs. *order-relevant* trials in occipital and parietal ROIs. MVPA was performed via L2-regularized logistic regression with a penalty term of 25, using the Princeton Multi-Voxel Pattern Analysis toolbox (www.pni.princeton.edu/mvpa/). The classifiers were trained and tested on the patterns corresponding to the two categories (i.e., context-relevant vs. *context-irrelevant* and *location-relevant* vs. *order-relevant*) at each time point (TR) through a leave-one-trial-out k-fold cross-validation procedure for each subject and ROI separately. We carried out two versions of the context-relevant vs. *context-irrelevant* MVPA. First, because there were twice as many context-relevant trials as *context-irrelevant* trials, we randomly selected half the *location-relevant* and half the *order-relevant* trials and trained a classifier to discriminate these context-relevant trials from *context-irrelevant* trials, then repeated this process 100 times and averaged performance across iterations to obtain a measure of classifier accuracy within the given ROI for each subject. In the second approach, one classifier was trained to decode *location-relevant* trials from *context-irrelevant* trials, and a second classifier was trained to decode *order-relevant* trials from

context-irrelevant trials. This approach allowed us to use all trials, summarizing classifier performance using the average performance of the two classifiers. Because the two approaches yielded nearly identical results, we report the results of the latter.

Classifier performance was summarized using the area under the curve (AUC). AUC reflects the sensitivity of the classifier in discriminating between the two categories and was computed as follows: We first selected a target category for each of the two classifiers and computed the proportion of hits vs. false alarms. The AUC was then computed using trapezoidal approximation to estimate the area based on these two proportions. An AUC greater than 0.5 indicates sensitivity to the target category. Statistical results were summarized through one-tailed one-sample *t*-tests comparing the classifier AUC against 0.5. False discovery rate (FDR) correction was used to correct the *p*-values for the 12 comparisons against chance level (i.e., at each TR) for a given ROI and classifier.

Hypothesis 3 formalized the idea that the representation of stimulus context in VWM is under strategic control, by positing differences in the strength of inverted encoding model (IEM) reconstruction of the neural representation of the location of the three sample items as a function of their relevance for retrieval from VWM. To test this, we used multivariate IEMs (Brouwer & Heeger 2009, Brouwer & Heeger 2011; Serences & Saproo 2012; Sprague & Serences 2013) to reconstruct channel tuning function (CTF) response profiles that track the perceived and remembered probe locations from multivoxel patterns of activity. IEMs were trained on sample-evoked signal (TR 4) from load-of-1 trials, labeled by location, and tested on load-of-3 trials. fMRI data from all trials (both correct and incorrect) were included in the IEM training and reconstruction. We extracted the normalized responses of each voxel in the *occipital-sample* ROI for each time point. The logic behind the method is that BOLD signal from each voxel can be

construed as a weighted sum of responses from six hypothetical channels optimally tuned for a specific stimulus location (i.e., 0 deg, 60 deg, 120 deg, 180 deg, 240 deg, and 300 deg). For each ROI, we estimated the set of weights that mapped each voxel's response to each location channel from the load-of-1trial training data set and then inverted this weight matrix to estimate channel responses for test data from each load-of-3 test trial. The average response output for each channel across trials was obtained by circularly shifting each response to a common center of 0°. The shifted channel outputs were averaged across all iterations in each subject. To quantify the resultant reconstructions of neural representations of stimulus location, we collapsed over channel responses on either side of the target channel (i.e., channel = 0° after shifting the outputs), averaged, and then used linear regression to estimate slope of the reconstruction for each subject at each tested TR. Finally, we computed the between-subjects average slope. A slope value greater than 0 can be interpreted as evidence for an active neural representation (Foster et al. 2017), and in these analyses slope served as a proxy for the strength of the representation. Statistical significance of the slope was assessed with a bootstrapping method (Ester et al. 2015, Ester et al. 2016). We randomly selected (with replacement) a set of reconstructions equal to the sample size and averaged them. This step was repeated 2500 times. We estimated the slope of each reconstruction, and a *p*-value was computed as the proportion of permutations for which the slope estimates were ≤ 0 for positive reconstructions. For negative reconstructions, the *p*-value was computed as 1 – the proportion of permutations for which the slope estimates were ≤ 0. Additionally, a 95% confidence interval for slope was constructed using the lower 2.5^{th} and upper 97.5^{th} percentiles of the bootstrapped distribution. Comparison of reconstruction slopes across trial types -- critical for the tests of our hypotheses – was carried out with two-sided paired-sample t-tests and Bayes factors.

To test the sub-hypotheses under *Hypothesis 3*, the IEM trained on the sample-evoked signal from the load-of-1 trials was used to reconstruct: (*Hyp. 3A*) the location of the probe (TRs 9 and 10); (*Hyp. 3B*) the location of the sample cued by the superimposed digit in the probe stimulus from TRs 9 and 10, (*Hyp. 3C*) the location of the sample that corresponded to neither the location of the probe nor the sample location cued by the superimposed digit, from TRs 9 and 10. Hyp. 3A operationalizes the assessment of the sensitivity of the processing of the physical properties of the probe (specifically, the encoding of its location) to strategy (i.e., the probe's location is not relevant on *order-relevant* and *context-irrelevant* trials). *Hyp. 3B* operationalizes a test of whether an item's context is reinstated when that item is cued for the recognition judgment. *Hyp. 3C* operationalizes a test of whether the context of all items in the memory set are reinstated nonspecifically (an outcome that would argue against the strategic control of stimulus context in VWM). Note that, because the results generally did not differ between TRs 9 and 10, we averaged the results for each subject to obtain a single reconstruction slope for visualization purposes.

Additional planned analyses

In addition to the hypothesis tests described above, we also planned several additional analyses that, although not directly testing the three sets of hypotheses that were the primary motivation for this work, could nonetheless provide further insight into the role of context-binding in VWM. Related to *Hypothesis 1*, we planned to carry out "*Additional, Hyp. 1*": whole-brain contrasts of delay-period activity for context-relevant trials versus *context-irrelevant* trials and for *location-relevant* versus *order-relevant* trials. The delay period was modeled in a GLM with 8s boxcar regressors spanning the delay period and convolved with a canonical hemodynamic response function (coded by trial type), and six nuisance regressors related to

movement-related artefacts. Parameter estimates for the delay-period regressors were calculated from the least mean squares fit of the model to the data. To test for statistical significance of differences between conditions, we first formed subject-specific contrast, then normalized the resulting contrast images to a standard Montreal Neurological Institute (MNI) space, then submitted the set of 15 images (one per subject) to AFNI's 3dttest++ with the input "-ClustSim", which carried out a permutation analysis to compute a cluster-size threshold for a given voxel-wise *p*-value threshold, such that the probability of any clusters surviving the dual thresholds is at some given level. Results are reported after applying a threshold of $p < 0.001$ uncorrected in conjunction with a prescribed cluster size of 775 voxels (context-relevant vs. *context-irrelevant*) / 628 voxels (*location-relevant* vs. *order-relevant*) to achieve $p < 0.05$ familywise error correction for multiple comparisons across the whole brain volume. (Due to an oversight, the preregistered analysis plan did not explicitly state that we also planned to carry out these analyses in IPS subregions. However, because the Methods section of the preregistered document does indicate that we would analyze the activity in the IPS subregions, and to improve narrative flow, we will report the results of these analyses from the IPS subregions immediately after the whole-brain results.)

For *Additional, Hyp. 2*, we planned to carry out whole-brain searchlight MVPA comparisons of context-relevant vs. *context-irrelevant* and *location-relevant* vs. *order-relevant* trial types. For these analyses, we used The Decoding Toolbox (TDT; Hebart et al. 2015) submitting the beta images resulting from GLMs similar to *Additional, Hyp 1*, with the exception that the models were re-fit to each run separately and spanned the 14-s time frame from sample through probe, resulting in a set of betas for each condition and run. We ran cross-validated leave-one-run-out searchlight decoding analyses, wherein a separate support vector machine was

built for each voxel, fitted to the beta values within a sphere with a radius of 3 voxels. This resulted in three-dimensional decoding accuracy maps in native space for each participant and analysis. (Decoding accuracy was calculated relative to chance level (i.e., 50% was subtracted from all accuracies)). These individual-subject maps were normalized into MNI space and, to identify significant classification performance, the set of 15 images (one from each subject) was submitted to AFNI's 3dttest++ with the input "-ClustSim". Results are reported after applying a threshold of $p < 0.0001$ uncorrected in conjunction with a prescribed cluster size of 219 voxels (context-relevant vs. *context-irrelevant*) / 217 voxels (*location-relevant* vs. *order-relevant*) to achieve $p < 0.05$ familywise error correction for multiple comparisons across the whole brain volume.

For *Additional, Hyp. 3,* we planned three analyses. (*i*) The first entailed repeating the analyses testing Hypothesis 3 but with IEMs trained on the probe-evoked signal (TRs 9 and 10) of load-of-3 trials, and labeled according to the location-on-the-screen of the probe. (*ii*) The second analysis used IEMs trained on the sample location-evoked signal (TR 4) from load-of-1 trials from the *occipital-sample* and *parietal-delay* ROIs, and tested on late delay-period signal (TR 6) within the same ROI from load-of-3 trials. (*iii*) The third analysis involved IEM of stimulus orientation (i.e., not location). IEMs were trained on sample-evoked signal (TR 4) from load-of-1 trials, labeled by sample orientation, and tested on each time point (TR) of the load-of-3 trials, labeled according to the to-be probed sample orientation.

Post hoc analyses

As described below, the results of the preregistered analyses testing *Hypothesis 3* were found to be difficult to interpret, but also motivated additional post hoc analyses. For *post hoc analysis 1,* the analyses comprised a modification of the late-delay period analysis used for

Additional, Hyp. 3 (ii), which involved training an IEM on the late-delay period signal (TR 6) from load-of-1 trials from the *occipital-sample* and *parietal-delay* ROI labeled by the sample location and testing on the signal from the load-of-3 trial types at the same TR.

For *post hoc analysis 2*, the analyses comprised a modification of the probe-period analysis used for *Additional, Hyp. 3 (i)* (i.e., leave-one-run-out cross-validation in which we trained and tested on the load-of-3 trial TRs 9 and 10). Whereas for *Additional, Hyp. 3* the training data were labeled according to the location-on-the-screen of the probe, for *post hoc analysis 2* we trained four IEMs, labeling the training data differently for each one: (i) $IEM_{post\ hoc\ 2\ \#1}$ – trained and tested on the probe's location on the screen; (ii) $IEM_{post\ hoc\ 2\ \#2}$ – trained and tested on the location of the item referenced by the superimposed digit in the probe stimulus (note that this analysis is undefined for the *context-irrelevant* trials, in which the superimposed digit ranged from 4-6); (iii) $IEM_{post\ hoc\ 2\ \#3}$ – trained and tested on the location of the item that was not cued by the probe stimulus (note that, for *context-irrelevant* trials, this includes all three sample locations); (iv) $IEM_{post\ hoc\ 2\ \#4}$ – trained and tested on the locations not occupied by a sample (there were three of these on every trial). These analyses were carried out in both the *occipital-sample* and *parietal-delay* ROIs. In the event that either $IEM_{post\ hoc\ 2\ \#2}$ or $IEM_{post\ hoc\ 2\ \#3}$ was successful, $IEM_{post\ hoc\ 2\ \#4}$ would serve as a control to confirm that this approach of training and testing would not be able to reconstruct, at TRs 9 and 10, the locations that had not been occupied by a sample item.

Results

Behavior

Recognition accuracy during fMRI scanning was significantly higher on load-of-1 than on load-of-3 trials ($t(14) = 15.121$, $p < .001$) and median reaction time was significantly faster on

load-of-1 than on load-of-3 trials (*exact binomial p* = 0.0074; two-tailed sign rank test). Within load-of-3 trial types, accuracy was significantly greater for *location-relevant* than for both *order-relevant* ($t(14) = 5.019$, $p < .001$) and *context-irrelevant* ($t(14) = 4.797$, $p < .001$) trials. Note that although accuracy on *context-irrelevant* trials did not differ statistically from chance ($t(14) = 1.470$, $p = .082$), it also did not differ statistically from accuracy on *order-relevant* trials ($t(14) = 0.899$, $p = .384$). Also within load-of-3 trial types, median reaction time was significantly slower for *order-relevant* trials than both *location-relevant* (*exact binomial p* = 0.0352) and *context-irrelevant* (*exact binomial p* = 0.0074) trials, and did not differ between *location-relevant* and *context-irrelevant* trials (*exact binomial p* = 1; **Figure 2**).

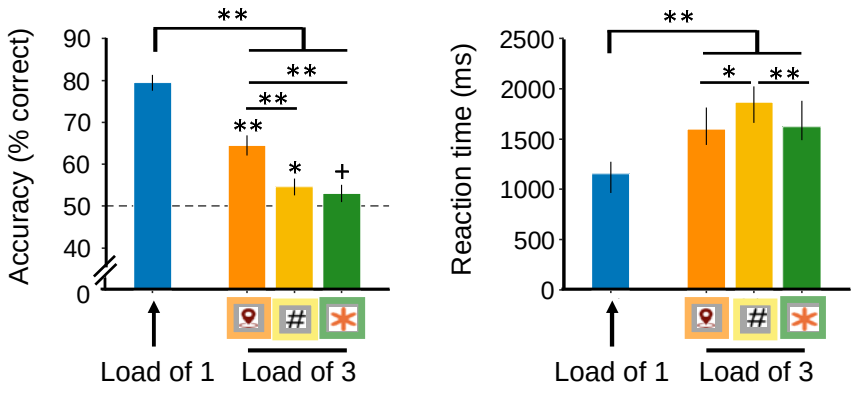

Figure 2. Behavioral results. Left panel: Accuracy as a function of trial type. Error bars correspond to +/- 1 standard error of the mean (SEM). Chance performance = 50% correct. Right panel: Reaction time as a function of trial type. Error bars correspond to bootstrapped 95% confidence intervals for the median. ** p < .01; * p < .05; + p < .1.

Hypothesis tests

Hypothesis 1A. The rationale for *Hypothesis 1A* was that activity in posterior parietal cortex remains elevated through the delay-period and appears to reflect, at least in part, context-

binding operations (Gosseries, Yu, et al. 2018; Cai et al. 2019; Cai et al. 2020). Univariate analyses of BOLD signal activity in the *parietal-delay* ROI confirmed the expected elevation of activity at the late delay-period TRs (6-7) for all trial types (all *t-statistics* ≥ *3.943,* all *p-values* < .002, all $BF_{10} \geq 27.806$; **Figure 3A**). Late delay-period activity was modulated by context-binding demands, with greater activity for context-relevant trials than *context-irrelevant* trials ($t(14) = 1.928$, $p = .037$, $BF_{10} = 2.187$) and load-of-1 trials ($t(14) = 3.717$, $p < .001$, $BF_{10} = 48749$). (Inspection of data from individual subjects revealed two subjects whose delay-period signal was an average of 0.21% greater for *context-irrelevant* than context-relevant trials. For the remaining subjects, this signal was an average of 0.13% greater on context-relevant than *context-irrelevant* trials ($t(12) = 3.717$, $p < .002$, $BF_{10} = 28.663$). This pattern was observed in three subregions of IPS, with significantly greater late-delay period activity for context-relevant trials than *context-irrelevant* trials in IPS 1-3 (all *t-statistics* ≥ 1.9039, all *p-values* ≤ .0388, all $BF_{10} \geq 2.1126$; remaining subregions all *t-statistics* ≤ 1.7105, all *p-values* ≥ .0546, all $BF_{10} \leq 1.6150$; **Figure 3C**). These results were consistent with *Hypothesis 1A.*

Hypothesis 1B. The rationale for *Hypothesis 1B* was that delay-period activity in occipital cortex returns to baseline and does not exhibit sensitivity to load or context-binding operations (Gosseries, Yu, et al. 2018; Cai et al. 2019; Cai et al. 2020). In the *occipital-sample* ROI, as predicted, delay-period BOLD activity did not differ from baseline for all trial types (all *t-statistics* ≤ 1.47, all *p-values* ≥ .1637, all $BF_{10} \leq 0.6406$). Furthermore, activity in all three of the load-of-3 trial types was greater than the activity in the load-of-1 trial type during the very early delay period (TR 4; all *t-statistics* ≥ 6.965, all *p-values* < .001, all $BF_{10} \geq 3201.7$; **Figure 3B**) but not at later time points. These results were consistent with *Hypothesis 1B.*

Hypothesis 1C. The rationale for *Hypothesis 1C* was to confirm, at the within-subject level, the observation across experiments that the patterns corresponding to *Hypotheses 1A* and *1B* are observed regardless of whether spatial location (Cai et al. 2020) or ordinal position (Gosseries, Yu, et al. 2018) is the task-critical domain of context. Consistent with *Hypothesis 1C*, no differences in delay-period activity were observed between the two context-relevant trial types, in the *occipital-sample* ROI (all *t-statistics* ≤ 0.465, all *p-values* ≥ .6755, all $BF_{10} \leq$ 0.1873), in the *parietal-delay* ROI (all *t-statistics* ≤ 0.4311, all *p-values* ≥ .4659, all $BF_{10} \leq$ 0.2747), or in any subregion of IPS (all *t-statistics* ≤ 0.5453, all *p-values* ≥ .5941, all $BF_{10} \leq$ 0.2990; **Figure 3C**).

Additional, Hyp 1. For the whole-brain analysis of delay-period activity, the context-relevant vs. *context-irrelevant* contrast revealed six clusters showing context-relevant > *context-irrelevant*– left precuneus, left superior parietal lobule, left IPS, left precentral gyrus, right cerebellum, and caudate nucleus bilaterally – and one cluster spanning left insula and superior temporal gyrus showing *context-irrelevant* > context-relevant (see **Figure 3D; Table 1**). For the *location-relevant* vs. *order-relevant* contrast, no clusters survived thresholding.

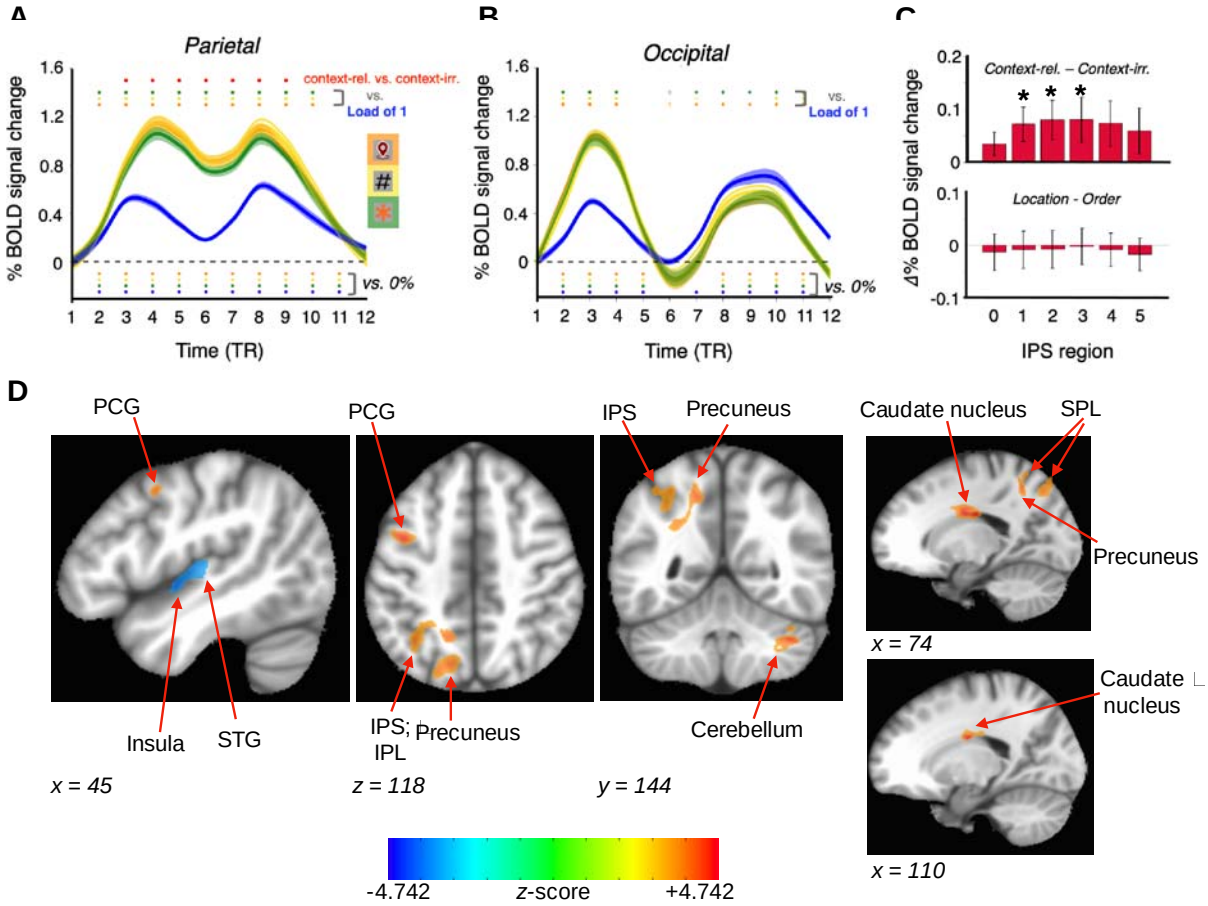

Figure 3. Univariate analysis results. **(A)** Percent BOLD signal change in the *parietal-delay* ROI at each TR for the load-of-1 (blue), *context-irrelevant* (green), *order-relevant* (yellow), and *location-relevant* (orange) trial types. Dark lines correspond to the mean at each time point; translucent ribbons correspond to +/- 1 SEM (time courses smoothed for visualization). Symbols below the dashed line indicate significance relative to baseline; symbols above the data indicate significant differences between conditions (note that *Hypothesis 1* relates to TRs 6-7). **(B)** Same format as **(A)** for the *occipital-sample* ROI. **(C)** Difference in BOLD signal change between the (Top) context-relevant and *context-irrelevant* trials types and (Bottom) *location-relevant* and *order-relevant* trial types during the late delay period (TRs 6-7) for individual subregions of IPS. Error bars correspond to +/- 1 SEM. * $p < .05$. **(D)** Clusters identified in a whole-brain analysis

contrasting delay-period activity for context-relevant vs. *context-irrelevant* trial types. Positive z-scores correspond to context-relevant > *context-irrelevant*; negative z-scores correspond to context-relevant < *context-irrelevant*.

Region	**Hemisphere**	**Peak voxel MNI coordinates (L,P,S)**	**Number of voxels**	**Z-score at peak**	**Direction of effect**
Precuneus; Superior parietal lobule	Left	-14, -56, -50	4522	4.668	Context-relevant > *Context-irrelevant*
Intraparietal sulcus; Inferior parietal lobule	Left	-40, -58, 52	1886	4.179	Context-relevant > *Context-irrelevant*
Caudate nucleus	Left	-18, -16, 26	1879	4.374	Context-relevant > *Context-irrelevant*
Caudate nucleus	Right	18, -8, 26	1789	4.598	Context-relevant > *Context-irrelevant*
Cerebellum	Right	40, -54, -36	1776	4.142	Context-relevant > *Context-irrelevant*
Insula; Superior temporal gyrus	*Left*	*-44, -6, -2*	*954*	*-3.964*	*Context-relevant < Context-irrelevant*
Precentral gyrus	Left	-40, 2, 46	921	4.545	Context-relevant > *Context-irrelevant*

Table 1. Regions identified in whole-brain contrast of delay-period activity for context-relevant vs. *context-irrelevant* trial types (see Figure 3.D).

Hypothesis 2. The rationale for *Hypothesis 2* was that brain areas associated with VWM should be sensitive to (*i*) the level of demand on context binding, and (*ii*) the informational domain of task-specific context. In the *parietal-delay* ROI, MVPA successfully classified context-relevant from *context-irrelevant* trials, building steadily from TR3 through the remainder the trial. In the *occipital-sample* ROI, the temporal profile of classifier performance was reversed – strongest early in the trial, then declining to chance levels during the late delay period (TR 7) and fluctuating thereafter; **Figure 4A**). Classification of *location-relevant* from *order-relevant* trials in the *parietal-delay* and *occipital-sample* ROIs followed qualitatively similar patterns (**Figure 4B**). These results, consistent with *Hypothesis 2*, suggest broad representation of stimulus context across areas supporting VWM.

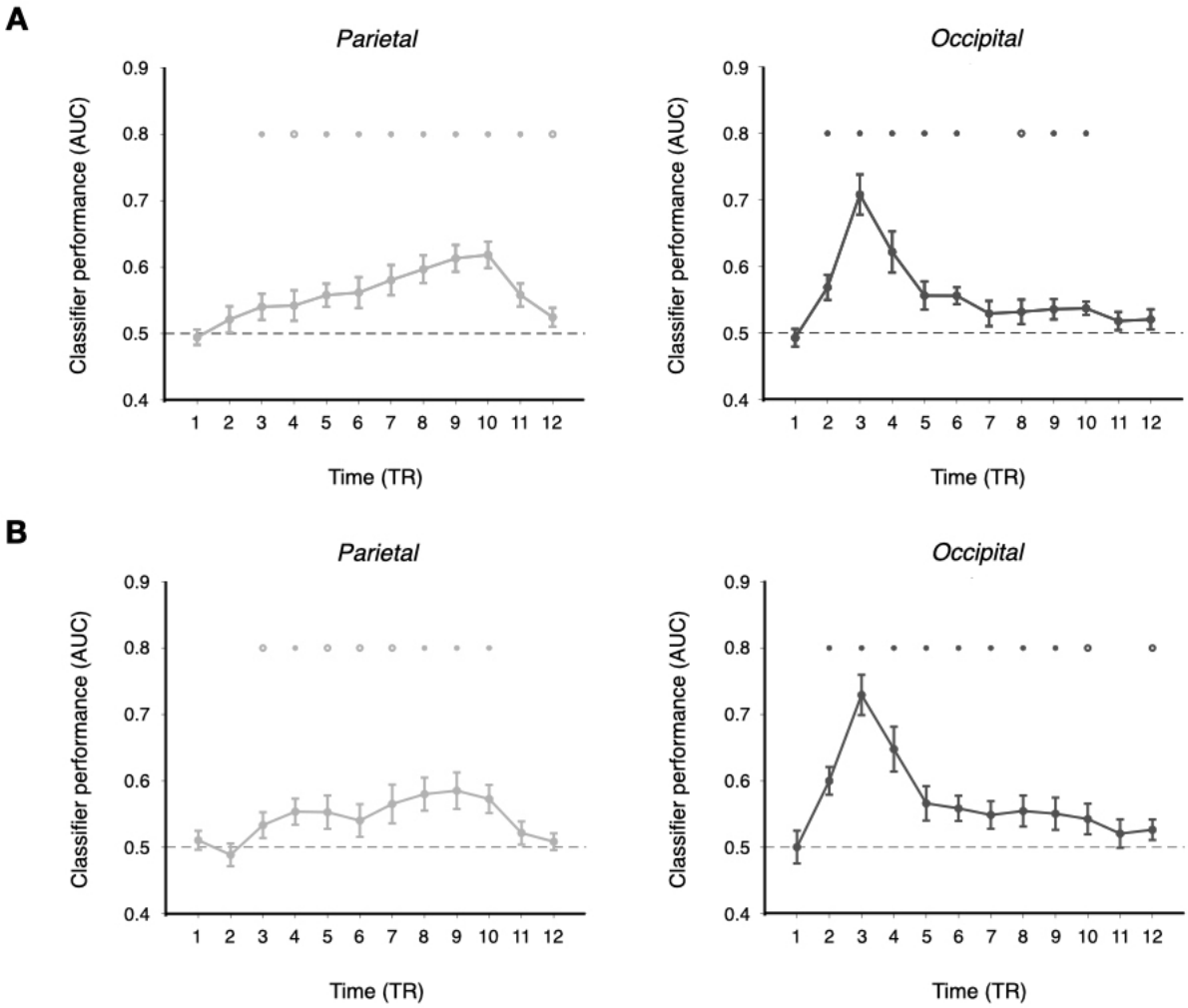

Figure 4. MVPA results. **(A)** Time course of classifier accuracy (AUC) in discriminating context-relevant from *context-irrelevant* load-of-3 trial types in the *parietal-delay* ROI (left) and *occipital-sample* ROI (right). **(B)** Time course of classifier accuracy (AUC) in discriminating *location-relevant* from *order-relevant* load-of-3 trials in the *parietal-delay* ROI (left) and *occipital-sample* ROI (right). Error bars correspond to +/- 1 SEM. Circular symbols indicate significance relative to chance level performance (0.5); solid symbols: fdr-corrected *p*-values < .05; open symbols: fdr-corrected *p*-values < .1.

Additional, Hyp. 2. The searchlight analysis, collapsing across the entirety of the trial, was able to discriminate context-relevant trials from *context-irrelevant* trials in areas that overlapped the *a priori* ROIs, as well as in several clusters in frontal cortex in both hemispheres, and in left anterior superior temporal gyrus (**Table 2**). For classification of *location-relevant* vs. *order-relevant* trials, the searchlight analysis identified clusters in a similarly broadly distributed set of regions (**Table 3**).

Region	Hemisphere	Peak voxel MNI coordinates (L,P,S)	Number of voxels	Z-score at peak
Inferior frontal gyrus; Middle frontal gyrus	Right	36, 24, 26	2102	5.003
Superior parietal lobule; Inferior parietal lobule; Postcentral gyrus	Right	30, -46, 48	794	4.838
Temporal pole; Superior temporal gyrus	Left	-49, 7, -8	407	5.236
Superior frontal gyrus; Superior middle gyrus	Right	15, 32, 49	376	4.829
Lateral intraparietal cortex	Left	-35, -68, 27	236	4.458
Extrastriate	Left	-37, 82, -3	221	4.647

Table 2. Regions identified by searchlight MVPA to discriminate context-relevant from *context-irrelevant* trial types.

Region	Hemisphere	Peak voxel MNI coordinates (L,P,S)	Number of voxels	Z-score at peak
V1	left	-3, -82, -8	508	4.908
Insula	Right	45, -4, 0	496	4.793
Superior frontal gyrus	Right	30, -8, 61	406	5.493
Middle temporal gyrus	Right	58, -47, -7	275	5.038
Inferior frontal gyrus	Left	-41, 18, 28	259	4.758
Superior parietal lobule	Left	-25, -49, 65	248	5.217

Table 3. Regions of significant searchlight classification accuracy of *location-relevant* from *order-relevant* trial types.

Hypothesis 3. Broadly, the rationale for this hypothesis was to explore the idea that the representation of stimulus context in VWM is under strategic control, with sub-hypotheses addressing the IEM reconstruction of the location of the different stimulus items: the location of the probe on the screen (*Hyp. 3A*); the location of the sample designated by the digit appearing

on the probe (*Hyp. 3B*); and the location of the sample not referenced by the probe (*Hyp. 3C*). *Hypothesis 3A* assessed the strength of the representation of the location of the probe on the screen, as a function of trial type. In the *occipital-sample* ROI, IEMs trained on the location of the sample from load-of-1 trials produced robust reconstructions of the location of the probe at TRs 9 and 10 for all three load-of-3 trial types (all bootstrapped *p*-values < .001; left panel of **Figure 5A**), and these effects did not differ by trial type (all *t*-statistics ≤ 1.9614, all *p*-values ≥ .07; all *BFs* ≤ 1.1881). This confirmed the prediction of *Hypothesis 3A* that the strength of the neural representation of the physical location of the probe would not vary as a function of trial type (i.e., as a function of the relevance of that information).

Hypotheses 3B and 3C. The goal of *Hypotheses 3B and 3C* was to assess context reinstatement in VWM: Is context reinstatement specific to the item being cued for the recognition judgment (*Hyp. 3B*), or is it nonspecific (i.e., is a representation of the location of all three sample stimuli reinstated; *Hyp. 3C*)? Importantly, the same encoding model was used for the analyses assessing *Hypotheses 3A-C*. Tests of *Hypothesis 3B* focused on IEM reconstructions of the location of the sample that was referenced by the digit superimposed on the probe stimulus. In the *occipital-sample* ROI, IEM reconstructions of the location of the digit-referred sample were significantly negative (all bootstrapped *p*-values ≤ .0228), and they did not differ between *location-relevant* and *order-relevant* trial types (t(14) = 0.8921, *p* = .2152, BF_{10} = 0.00004). Therefore, they were opposite in sign relative to, and significantly different from, the reconstructions of the physical location of the probe (i.e., results for *Hyp. 3A*; all *t*-statistics ≥ 5.3097, all *p*-values < .001; all *BFs* ≥ 231.3) The tests of *Hypothesis 3C* focused on IEM reconstructions of the location of the sample that did not correspond to either the location-on-the-screen of the probe or the probe's digit. For this item, the slopes of the reconstructions of its

location were, again, significantly negative (all bootstrapped *p*-values < .001). Additionally, they were significantly more negative on *order-relevant* trials than on *location-relevant* trials ($t(14) = 2.5633$, $p = .0225$, $BF_{10} = 2.8798$), with no other differences observed (middle and right panels of **Figure 5A**). We found the same qualitative pattern of results with *Additional, Hyp. 3(i)*, in which we repeated the analyses but trained the model on the probe-evoked signal (TRs 9 and 10) from the load-of-3 trial types (results not shown). The negative reconstructions generated in the tests of *Hypotheses 3B and 3C* and *Additional, Hyp. 3(i)* are almost surely due to the fact that activity in the *occipital-sample ROI* during the probe/response period of the trial was dominated by the visual drive of the probe stimulus on the screen. This made them ill-suited for testing the encoding of locations other than that of the probe (*Hypotheses 3B and 3C),* including with the model trained on the location of the probe and tested on other locations. Although this renders the results from these tests difficult to interpret, it also gave us an idea for an alternative approach, described below as *post hoc analysis 2*.

For *Additional, Hyp. 3(ii),* we were unable to reconstruct the location of any sample item during the late delay period, in either the *occipital-sample* or the *parietal-delay* ROI (all bootstrapped *p*-values ≥ .0744). For *Additional, Hyp. 3(iii),* we were unable to reconstruct orientation in any of the conditions at any time point. The failure to reconstruct orientations in the current experiment might be due to a mixture effect of the large number of orientations presented on each trial and the peripheral presentation of orientations.

Post hoc analyses. Post hoc analysis 1 revealed significant positive reconstruction of the location of the to-be probed sample item during the late delay period (TRs 6 and 7) in the *occipital-sample ROI* for *location-relevant* trials only (both bootstrapped *p*-values ≤ .0104; all

other bootstrapped *p*-values ≥ .0516 for reconstructions for other trial types and reconstructions in the *parietal-delay* ROI).

Post hoc analysis 2 addressed the question of context reinstatement at the time of the probe by training four IEMs on data from TRs 9 and 10, each labeled according to the location of a different sample item. The results in the *occipital-sample* ROI produced significantly positive reconstructions of the location of the probe on the screen (on all three trial types; $IEM_{post\ hoc\ 2\ \#1}$), of the location of the digit-cued item (on both *location-relevant* and *order-relevant* trials; $IEM_{post\ hoc\ 2\ \#2}$), and of the location of the uncued item(s) (the uncued item on *location-relevant* and *order-relevant* trials, and all three locations on *context-irrelevant* trials; $IEM_{post\ hoc\ 2\ \#3}$) (all bootstrapped *p*-values < .02; **Figure 5B**). The interpretability of these results was reinforced by the failure of $IEM_{post\ hoc\ 2\ \#4}$ to reconstruct, at TRs 9 and 10, the locations that had not been occupied by a sample (all bootstrapped *p*-values ≥ .4364; **Figure 5C)**. Together, the results from *post hoc analysis 2* suggest that, at test, the locations of all sample items from that trial were reactivated, regardless of whether or not they corresponded to the item being probed.

In the *parietal-delay* ROI, results for $IEM_{post\ hoc\ 2\ \#1}$ revealed significant positive reconstruction of the location-on-the-screen of the probe for all three trial types (all bootstrapped *p*-values < .002), with the slope of the reconstruction during *order-relevant* trials numerically lower than during the other two trial types, and significantly so for *context-irrelevant* trials ($t(14) = 2.6459$, $p = .0192$; $BF_{10} = 3.2771$). Results for $IEM_{post\ hoc\ 2\ \#2}$ revealed a significant *negative* reconstruction of the location of the digit-referenced item on *location-relevant* trials (bootstrapped *p*-value = .0048), an effect that differed significantly from its reconstruction on *order-relevant* trials ($t(14) = 2.2801$, $p = .0388$; $BF_{10} = 1.8725$). For $IEM_{post\ hoc\ 2\ \#3}$ and $IEM_{post\ hoc\ 2\ \#4}$, no reconstructions were observed (all bootstrapped p-values ≥ 0.4336; **Figure 5D**).

Therefore, the patterns from the *parietal-delay* ROI differ markedly from those in the *occipital-sample* ROI, suggesting that the latter may play a role in deemphasizing irrelevant information during test (i.e., the location of the order-referred item on *location-relevant* trials, and the location of the location-referred item on *order-relevant* trials).

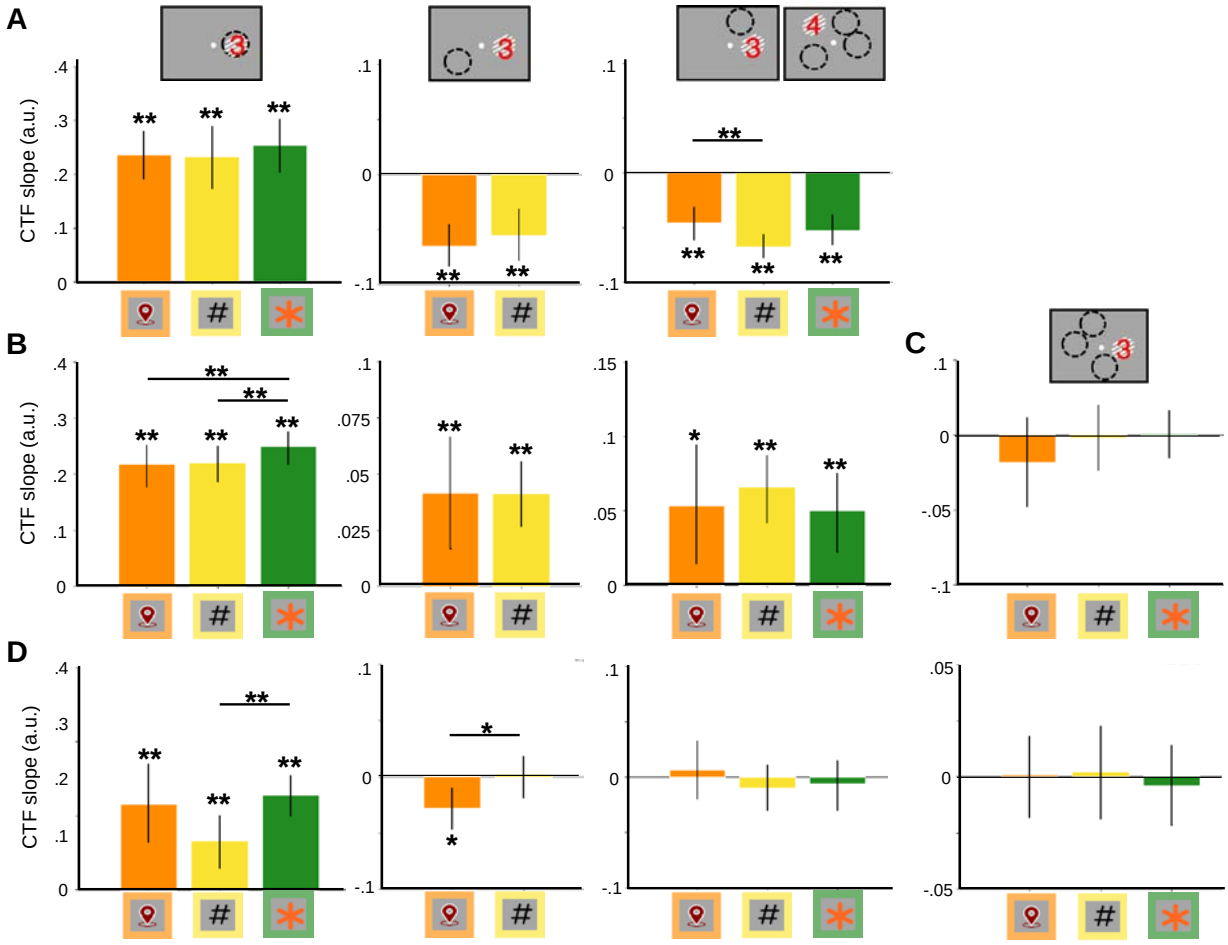

Figure 5. Slopes of IEM reconstructions of location information from the probe-evoked signal. The illustrations of the probe display at the top of each column indicate the location (dashed circle) reconstructed by the IEM (c.f., Fig. 1): that of the item that appeared at the same location as the probe (left-hand column); that of the item referenced by the digit superimposed on the orientation patch (second from left-hand column; that of the item unreferenced by the probe

(third from left-hand column); or one of the locations that was not occupied by a sample on that trial (panel C and right-hand column of panel D) Symbols along the horizontal axis of each plot indicate the trial type on which the IEM is being tested. (Note that for the second column from the left, data from context-irrelevant trials could not be used because the probe on these trials was superimposed with a digit ("4", "5", or "6") that did not refer to a location at which a sample had appeared.) **(A)** *Hypothesis 3: Occipital-sample* ROI, IEMs trained on sample-evoked activity (TR 4) from load-of-1 trials: slopes of the reconstructions (CTFs) of the tested sample location during the load-of-3 trial type indicated by the symbol along the horizontal axis. **(B)** $IEM_{post\ hoc\ 2\ \#s\ 1\text{-}3}$ (i.e., using models trained and tested on data from TRs 9 and 10 from load-of-3 trials), *occipital-sample* ROI. Left panel ($IEM_{post\ hoc\ 2\ \#1}$): Slopes of the reconstructions with a model trained and tested on the physical location of the probe. Central panel ($IEM_{post\ hoc\ 2\ \#2}$): Slopes of the reconstructions with a model trained and tested on the digit-referenced sample location. Right panel ($IEM_{post\ hoc\ 2\ \#3}$): Slopes of the reconstructions with a model trained and tested on the unreferenced sample location. **(C)** $IEM_{post\ hoc\ 2\ \#4}$, o*ccipital-sample* ROI: Slopes of reconstructions with a model trained and tested on locations that were not occupied by a sample on that trial. **(D)** $IEM_{post\ hoc\ 2\ \#s\ 1\text{-}4}$, *parietal-delay* ROI: Reconstructions using the same procedures as **(B)** and **(C)**. Error bars correspond to bootstrapped 95% confidence intervals. "*" and "**" above the individual bars correspond to bootstrapped *p*-values < .05 & < .01, respectively. "*"

Discussion

Context plays a critical role in working memory when situations require memory for where and/or when an item was encountered. Recent research has identified sensitivity to

context-binding demands in the delay-period activity of IPS (Gosseries, Yu, et al. 2018; Cai et al. 2019; Cai et al. 2020), indicating a role above and beyond that of item representation (Todd & Marois 2004, Todd & Marois 2005; Xu & Chun 2006). The results presented here replicate this evidence for context-binding sensitivity of IPS, and extend it to a task in which all sample items were drawn from the same category, sample displays were identical across trials, and the informational domain of trial-critical context varied on a trial-by-trial basis. In IPS, delay-period activity was higher for context-relevant than *context-irrelevant* trials, although it did not differ between *location-relevant* and *order-relevant* trials. Exploratory whole-brain univariate analyses revealed differences in delay-period activity for context-relevant and *context-irrelevant* trials in several clusters in parietal and frontal cortex, as well as in the cerebellum and basal ganglia, with no differences observed for *location-relevant* and *order-relevant* trials. Nevertheless, MVPA indicated that patterns of activity distinguished location context from order context in (a priori-defined) parietal and occipital ROIs, although the time courses differed in these two regions. Decoding was strongest in occipital cortex for the presentation of the trial-initiating instructional cue, then relatively weak for the remainder of the trial, whereas in parietal cortex, decoding began at chance levels, then slowly increased in strength across the duration of the trial. This was true for both context-relevant vs. *context-irrelevant* and *location-relevant* vs. *order-relevant* comparisons. Additionally, exploratory searchlight analyses revealed regions of above-chance decoding of context information in several clusters in temporal, parietal, and frontal cortex. These results together highlight an important role of parietal cortex, including IPS, in context binding in working memory.

Turning to IEM analyses, in occipital cortex there was exploratory evidence that, only on *location-relevant* trials, the representation of stimulus location returned to an active state late in

the delay period. This would be consistent with an anticipatory reactivation of the location context of the items being held in VWM, but only on trials when this information was needed to correctly interpret the probe. A few seconds later, however, when the recognition probe was on the screen, the locations at which all three items had been presented were actively represented (**Fig. 5B**), with only minimal evidence of modulation as a function of trial relevance. In parietal cortex, in contrast, only the location-on-the-screen of the probe stimulus was strongly represented during all trial types. Furthermore, on *location-relevant* trials, the representation of the digit-referred item (irrelevant on these trials) was suppressed significantly below baseline. These analyses with IEM provide insights about the dynamics and control of the representation of context in VWM, to which we now turn.

In occipital cortex, the fact that the locations of each of the three samples were actively represented during the probe epoch, on all three trial types, provides evidence for the automatic reinstatement of the location context of all items currently in VWM, regardless of the relevance of this information for selecting the item cued by the probe. This evidence for an automatic reinstatement of location context is consistent with previous evidence for the incidental encoding of location information, regardless of its task relevance (e.g., Ellis 1990; Treisman & Zhang 2006; Clark et al. 2012; Kondo & Saiki 2012; Foster et al. 2017; Cai et al. 2019; Heuer & Rolfs 2021). In addition to the putatively automatic activation of location that accompanies probe onset, our data also showed evidence that this information can be, selectively, perhaps strategically, activated in advance of probe onset, on trials when it will be needed for the recognition decision. Importantly, the failure to find these effects with IEMs trained on sample location from load-of-1 trials suggests that the neural code representing reinstated location

context late in the delay period differs from that representing the sensory representation of the perceived location of an item on the screen.

When we consider behavioral performance, it seems likely that part of the superiority of *location-relevant* trials relative to the other two trial types is a ‘same-position’ advantage (Hollingworth 2007; Sapkota et al. 2011). Additionally, however, the neural evidence for the probe-triggered activation of the location context of all items during *order-relevant* and *context-irrelevant* trials suggests the possibility that performance on these trials may also have suffered from interference from this trial-irrelevant information. Additional research with a procedure similar to the one used here, but testing recall instead of recognition, will be needed to explore whether the trial-irrelevant representation of location context may degrade performance on *order-relevant* and *context-irrelevant* trials.

Turning now to parietal cortex, the results of IEM analyses in this ROI were markedly different from those in occipital cortex (compare **Fig. 5B** vs. **5D**), and were more consistent with a role in filtering or weighting information according to its relevance for behavior (c.f., Zelinsky & Bisley 2015). In particular, neither the location of the item referenced by the superimposed digit (on *location-relevant* trials and *order-relevant* trials), nor those of the sample items presented on *context-irrelevant* trials, showed evidence of active reinstatement. Indeed, the IEM reconstruction of the location of the digit-referred item had a negative slope on *location-relevant* trials, a pattern opposite of its reconstruction on these same trials in occipital cortex. This specific result suggests a function of deemphasizing an item whose representation might otherwise interfere with the recognition decision. (In other research, similar patterns of "negative" IEM reconstruction have been associated with items that are either to be deprioritized

(Yu, Teng, & Postle 2020; Wan et al. 2020; Wan et al. 2022), or dropped (Lorenc et al. 2020) from VWM.

We note that our study was not designed to provide evidence for active selection, as might be expected from an IPS-based priority map (e.g., Bisley & Goldberg 2010; Jerde et al. 2012; Bisley & Mirpour 2019). One limitation of our study is that the lack of an a priori model of how sequential order is represented in the brain, particularly with a code that would be discriminable with fMRI, prevented us from carrying out an analysis comparable to the IEM analyses exploring the representation of location context. Thus, an open question for future research is whether it might be possible to find neural evidence that ordinal context may also be obligatorily encoded in VWM (Heuer & Rolfs 2021), and similarly flexibly prioritized according to task-specific demands.

Citation diversity statement

To promote transparency surrounding citation practice (Dworkin et al. 2019; Zurn et al. 2020) and mitigate biases leading to under-citation of work led by women relative to other papers in demonstrated across several scientific domains (e.g., Dworkin et al. 2019; Maliniak et al. 2013; Caplar et al. 2017; Fulvio et al. 2021), we proactively aimed to include references that reflect the diversity of the field and quantified the gender breakdown of citations in this article according to the first names of the first and last authors using the Gender Citation Balance Index web tool (https://postlab.psych.wisc.edu/gcbialyzer/) with manual correction as needed. This article contains 52.9% man/man, 5.9% man/woman, 32.4% woman/man and 8.8% woman/woman citations. For comparison, proportions estimated from articles in five prominent neuroscience journals (as reported in Dworkin et al. 2019) are 58.4% man/man, 9.4% man/woman, 25.5% woman/man and 6.7% woman/woman. Note that the estimates may not

always reflect gender identity and do not account for intersex, non-binary, or transgender individuals.

Acknowledgements

We thank Joshua Chung for assistance with subject recruitment and behavioral screening.

Funding

This work was supported by National Institutes of Health grant R01MH064498 to B.R.P.

The authors declare no competing financial interests.

References

Bettencourt, K. C., & Xu, Y. (2016). Decoding the content of visual short-term memory under distraction in occipital and parietal areas. *Nature neuroscience*, *19*(1), 150-157. https://doi.org/10.1038/nn.4174

Bisley, J. W., & Goldberg, M. E. (2010). Attention, intention, and priority in the parietal lobe. Annual review of neuroscience, 33, 1-21. https://doi.org/10.1146/annurev-neuro-060909-152823

Bisley, J. W., & Mirpour, K. (2019). The neural instantiation of a priority map. *Current opinion in psychology*, *29*, 108-112. https://doi.org/10.1016/j.copsyc.2019.01.002

Brainard, D. H., & Vision, S. (1997). The psychophysics toolbox. *Spatial vision*, *10*(4), 433-436. https://doi.org/10.1163/156856897x00357

Cai, Y., Sheldon, A. D., Yu, Q., & Postle, B. R. (2019). Overlapping and distinct contributions of stimulus location and of spatial context to nonspatial visual short-term memory. *Journal of neurophysiology*, *121*(4), 1222-1231. https://doi.org/10.1152/jn.00062.2019

Cai, Y., Fulvio, J. M., Yu, Q., Sheldon, A. D., & Postle, B. R. (2020). The role of location-context binding in nonspatial visual working memory. *Eneuro*, *7*(6). https://doi.org/10.1523/ENEURO.0430-20.2020

Caplar, N., Tacchella, S., & Birrer, S. (2017). Quantitative evaluation of gender bias in astronomical publications from citation counts. *Nature astronomy*, *1*(6), 1-5. https://doi.org/10.1038/s41550-017-0141

Clark, K. L., Noudoost, B., & Moore, T. (2012). Persistent spatial information in the frontal eye field during object-based short-term memory. Journal of Neuroscience, 32(32), 10907-10914. https://doi.org/10.1523/JNEUROSCI.1450-12.2012

Cox, R. W. (1996). AFNI: software for analysis and visualization of functional magnetic resonance neuroimages. *Computers and Biomedical research*, *29*(3), 162-173. https://doi.org/10.1006/cbmr.1996.0014

Dworkin, J. D., Linn, K. A., Teich, E. G., Zurn, P., Shinohara, R. T., & Bassett, D. S. (2020). The extent and drivers of gender imbalance in neuroscience reference lists. *Nature neuroscience*, *23*(8), 918-926. https://doi.org/10.1038/s41593-020-0658-y

Ellis, N. R. (1990). Is memory for spatial location automatically encoded?. *Memory & Cognition*, *18*(6), 584-592. https://doi.org/10.3758/BF03197101

Foster, J. J., Bsales, E. M., Jaffe, R. J, & Awh, E. (2017). Alpha-band activity reveals spontaneous representations of spatial position in visual working memory. *Current Biology*, *27*, 3216–3223.e6, 2017. https://doi.org/10.1016/j.cub.2017.09.031

Fulvio, J. M., Akinnola, I., & Postle, B. R. (2021). Gender (im) balance in citation practices in cognitive neuroscience. *Journal of Cognitive Neuroscience*, *33*(1), 3-7. https://doi.org/10.1162/jocn_a_01643

Gosseries, O., Yu, Q., LaRocque, J. J., Starrett, M. J., Rose, N. S., Cowan, N., & Postle, B. R. (2018). Parietal-occipital interactions underlying control-and representation-related processes in working memory for nonspatial visual features. *Journal of Neuroscience*, *38*(18), 4357-4366. https://doi.org/10.1523/JNEUROSCI.2747-17.2018

Hebart, M. N., Görgen, K., & Haynes, J.-D. (2015). The Decoding Toolbox (TDT): a versatile software package for multivariate analyses of functional imaging data. Frontiers in Neuroinformatics, 8(January), 1–18. https://doi.org/10.3389/fninf.2014.00088

Heuer, A., & Rolfs, M. (2021). Incidental encoding of visual information in temporal reference frames in working memory. *Cognition*, *207*, 104526. https://doi.org/10.1016/j.cognition.2020.104526

Hollingworth, A. (2007). Object-position binding in visual memory for natural scenes and object arrays. *Journal of Experimental Psychology: Human Perception and Performance*, *33*(1), 31. https://doi.org/10.1037/0096-1523.33.1.31

Jerde, T. A., Merriam, E. P., Riggall, A. C., Hedges, J. H., & Curtis, C. E. (2012). Prioritized maps of space in human frontoparietal cortex. *Journal of Neuroscience*, *32*(48), 17382-17390. https://doi.org/10.1523/JNEUROSCI.3810-12.2012

Kleiner, M., Brainard, D., & Pelli, D. (2007). What's new in Psychtoolbox-3?.

Kondo, A., & Saiki, J. (2012). Feature-specific encoding flexibility in visual working memory. *PloS one*, *7*(12), e50962. https://doi.org/10.1371/journal.pone.0050962

Lorenc, E. S., Vandenbroucke, A. R., Nee, D. E., de Lange, F. P., & D'Esposito, M. (2020). Dissociable neural mechanisms underlie currently-relevant, future-relevant, and discarded working memory representations. *Scientific reports*, *10*(1), 1-17. https://doi.org/10.1038/s41598-020-67634-x

Maliniak, D., Powers, R., & Walter, B. F. (2013). The gender citation gap in international relations. *International Organization*, *67*(4), 889-922. https://doi.org/10.1017/S0020818313000209

Pelli, D. G., & Vision, S. (1997). The VideoToolbox software for visual psychophysics: Transforming numbers into movies. *Spatial vision*, *10*, 437-442. https://doi.org/10.1163/156856897x00366

Sapkota, R. P., Pardhan, S., & van der Linde, I. (2011). Object—Position Binding in Visual Short-Term Memory for Sequentially Presented Unfamiliar Stimuli. *Perception*, *40*(5), 538-548. https://doi.org/10.1068/p6899

Todd, J. J., & Marois, R. (2004). Capacity limit of visual short-term memory in human posterior parietal cortex. *Nature*, *428*(6984), 751-754. https://doi.org/10.1038/nature02466

Todd, J. J., & Marois, R. (2005). Posterior parietal cortex activity predicts individual differences in visual short-term memory capacity. *Cognitive, Affective, & Behavioral Neuroscience*, *5*(2), 144-155. https://doi.org/10.3758/CABN.5.2.144

Treisman, A., & Zhang, W. (2006). Location and binding in visual working memory. *Memory & cognition*, *34*(8), 1704-1719. https://doi.org/10.3758/BF03195932

van Loon, A. M., Olmos-Solis, K., Fahrenfort, J. J., & Olivers, C. N. (2018). Current and future goals are represented in opposite patterns in object-selective cortex. *ELife*, *7*: e38677. https://doi.org/10.7554/eLife.38677

Wan, Q., Cai, Y., Samaha, J., & Postle, B. R. (2020). Tracking stimulus representation across a 2-back visual working memory task. *Royal Society open science*, *7*(8), 190228. https://doi.org/10.1098/rsos.190228

Wan, Q., Menendez, J. A., & Postle, B. R. (2022). Priority-based transformations of stimulus representation in visual working memory. *PLOS Computational Biology*, 18(6), e1009062. https://doi.org/10.1371/journal.pcbi.1009062

Xu, Y. (2017). Reevaluating the sensory account of visual working memory storage. *Trends in Cognitive Sciences*, *21*(10), 794-815. https://doi.org/10.1016/j.tics.2017.06.013

Xu, Y., & Chun, M. M. (2006). Dissociable neural mechanisms supporting visual short-term memory for objects. *Nature*, *440*(7080), 91-95. https://doi.org/10.1038/nature04262

Yu, Q., Teng, C., & Postle, B. R. (2020). Different states of priority recruit different neural representations in visual working memory. *PLoS biology*, *18*(6), e3000769. https://doi.org/10.1371/journal.pbio.3000769

Zelinsky, G. J., & Bisley, J. W. (2015). The what, where, and why of priority maps and their interactions with visual working memory. *Annals of the new York Academy of Sciences*, *1339*(1), 154-164. https://doi.org/10.1111/nyas.12606

Zurn, P., Bassett, D. S., & Rust, N. C. (2020). The citation diversity statement: a practice of transparency, a way of life. *Trends in Cognitive Sciences*, *24*(9), 669-672. https://doi.org/10.1016/j.tics.2020.06.009